Journal of Magnetic Resonance **157,** 17–30 (2002)
doi:10.1006/jmre.2002.2552

The Application of MAS Recoupling Methods in the Intermediate Motional Regime

Kay Saalwächter*,[1] and Ingrid Fischbach†

*Institut für Makromolekulare Chemie, Universität Freiburg, Stefan-Meier-Str. 31, D-70104 Freiburg, Germany; and †Max-Planck-Institute for Polymer Research, Ackermannweg 10, D-55128 Mainz, Germany

Received October 18, 2001; revised April 26, 2002

We present investigations concerning the effect of molecular motions on the experimental timescale upon the recoupling of anisotropic interactions under magic-angle spinning conditions. An approach for the efficient simulation of spin dynamics occurring during complex pulse sequences, based on a linearization of the general solution of the stochastic Liouville–von Neumann equation, was developed. Using ^{13}C CSA recoupling of the methyl carbon in dimethylsulfon as a sample interaction, we observed a characteristic signal decay under recoupling upon entering the intermediate motional regime, which can be well described by an apparent transverse relaxation time, T_2^{rcpl}. This quantity does not depend on the spinning frequency to a first approximation. Specific recoupling experiments, namely the measurement of tensor parameters by spinning sideband analysis, and the determination of rate constants with the CODEX experiment, are discussed with respect to possibilities and limits of their application in the intermediate motional regime. Important conclusions are drawn with regards to the limited applicability of popular recoupling methods like REDOR to samples exhibiting intermediate mobility.

Key Words: **magic-angle spinning; recoupling; simulations; dynamics; REDOR.**

1. INTRODUCTION

High-resolution magic-angle spinning (MAS) NMR has evolved into a uniquely versatile tool for the elucidation of structure and dynamics in solid materials (*1*). Particularly, a dramatic simplification of the spectra can be achieved by very-fast MAS with spinning frequencies exceeding 15 kHz, whereupon the influence of most anisotropic interactions among spin-$\frac{1}{2}$ nuclei on the spectra, in particular strong dipolar couplings among protons, can be suppressed to such a degree that the resolution needed to tackle complex multispin systems is attained. By means of recoupling, i.e., the application of specifically designed rotor-synchronized pulse sequences (*2*), specific anisotropic interactions can be selectively reintroduced, thus providing very specific information on orientation-dependent phenomena. Recoupling methods represent a very powerful and indispensable part of the modern NMR toolbox (*3, 4*). Most of the numerous recent applications are focused on structural issues, with dynamics being considered a complication to be avoided. If the exchange process is *fast* on the experimental timescale, recoupling methods may straightforwardly be used to extract dynamically averaged tensor parameters, by means of which the geometry of the process and the associated order (often characterized by a dynamical order parameter) can be assessed. An instructive example may be found in (*5*). In the other extreme, recoupling exchange methods, which are specifically designed to probe *slow* motional processes on a ms-s timescale, have been presented. In this case, recoupling is used to measure tensor parameters of, e.g., the ^{13}C chemical shift anisotropy (CSA) (*6, 7*) or ^{13}C–^{13}C dipolar interactions (*8*) before and after a long mixing time, during which the slow motional processes may occur.

Despite the possible complications associated with intermediate motions, recent applications have also emerged in the field of polymer dynamics (*9, 10*), where residual ^{1}H–^{1}H homonuclear dipolar couplings characterizing the local dynamic order parameter of polymer chains in entangled melts were measured by using double-quantum MAS recoupling methods. Importantly, a polymer melt is characterized by various dynamic processes occurring on very different timescales spanning the whole range from fast-limit averaging to slow exchange, with ample contributions also in the intermediate region. An assumption implicit to the authors' analysis of the data in terms of scaling laws is that these timescales are well separated, i.e., that spin correlations are only observed which depend on a dipolar interaction which is on the one hand averaged in the fast limit by one process, but is not yet substantially influenced further by motions on the experimental timescale or slower. An understanding of the underlying effects will likely contribute to establish a more complete picture of the interplay of polymer dynamics and the new NMR experiments.

There exists ample theoretical and experimental work in support of the assumption that any motional process on the timescale of a MAS experiment should lead to an efficient suppression of the signal of segments with intermediate mobility (*11–14*). However, a specific treatment of intermediate motions occurring during recoupling seems to be missing. This paper is intended as a first approach to fill this gap. We present results of numerical

[1] To whom correspondence should be addressed.

1090-7807/02 $35.00

simulations and experimental data on a well-characterized model system, dimethyl sulfone, in which the two methyl groups are known to switch their position by a simple Arrhenius-activated two-site jump process (*15, 16*). We restrict our attention to the ^{13}C CSA tensor, as recoupled by a simple train of rotor-synchronized π-pulses spaced by half a rotor period. This recoupling scheme, originally introduced by Gullion and Schaefer for heteronuclear dipolar couplings under the name REDOR (*17*), and later applied to CSA recoupling by Hong (*18*) and Schmidt-Rohr (*7*), represents one of the simplest approaches to recoupling: the π pulses cause a change in the sign of the spin part of the interaction Hamiltonian acting during every other half rotor period; this exactly compensates for the change in the sign of the MAS-modulated space part of the interaction Hamiltonian. In this way, the averaging of the total Hamiltonian to zero by MAS is avoided.

It is shown that the recoupling process itself leads to a very selective loss in signal from regions associated with intermediate reorientations of the recoupled interaction tensor. This decay is phenomenologically well described by an apparent transverse relaxation time T_2^{rcpl}, which in the special case presented here has a very simple dependence upon the rate constant of the process. We will discuss the implications and the possible use of this phenomenology.

2. THEORETICAL BACKGROUND

CSA recoupling. For a spin exhibiting a CSA, the ω_R-dependent interaction frequency is given by

$$\omega(t) = C_1\cos(\gamma+\omega_R t) + C_2\cos(2\gamma+2\omega_R t) + S_1\sin(\gamma+\omega_R t) + S_2\sin(2\gamma+2\omega_R t), \quad [1]$$

where the coefficients $C_{1,2}$ and $S_{1,2}$ depend on the interaction parameters δ, η and on the angles α and β (*19*). The complete set of Euler angles α, β, γ relates the orientation of the principal axes system of the CSA tensor to the rotor-fixed frame. Free evolution of transverse ^{13}C magnetization during an interval $(t_a; t_b)$ leads to a phase factor

$$\Phi(t_a; t_b) = \int_{t_a}^{t_b} \omega(t)\,\mathrm{d}t. \quad [2]$$

This integral is equal to zero when $t_b - t_a = n\tau_R$ (no recoupling). When π-pulses are applied every $\frac{1}{2}\tau_R$ for a total of $\frac{N}{2}$ rotor periods, as done in the experiment in Fig. 1a, a nonvanishing total phase of

$$\frac{N}{2}\bar{\Phi}(t) = \frac{N}{2}2\int_{t}^{\tau_R/2+t}\omega(t)\,\mathrm{d}t = \frac{N}{2}\left(4\frac{S_1}{\omega_R}\cos(\gamma+\omega_R t) - 4\frac{C_1}{\omega_R}\sin(\gamma+\omega_R t)\right) \quad [3]$$

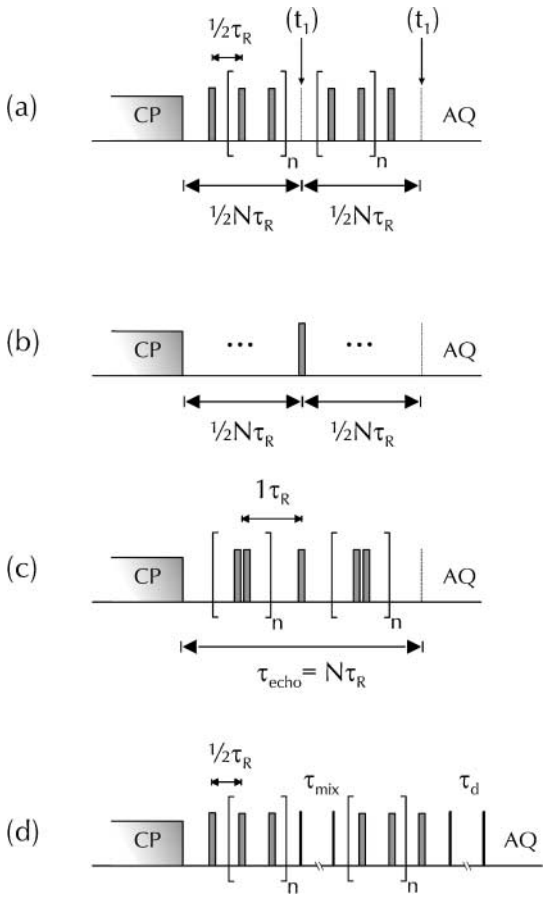

FIG. 1. Pulse sequences for recoupled echo (a) and reference experiments (b, c), as discussed in the text. The ^{1}H channel pulses (preparation, CP, and decoupling) are omitted for clarity. The sequence in (d) represents the CODEX experiment (*6*). In (a), arrows indicate where incremented t_1 delays have to be inserted, such that the pulse sequence corresponds to the two-dimensional CSA sideband experiment (*18*), for which a z-filter is additionally implemented before acquisition.

is acquired. The parameter t is the starting time of the π-pulse train and can be set to $t = 0$ for a completely rotor-synchronized experiment. Its significance in rotor-asynchronous pulse sequences will be discussed below. The phase $\bar{\Phi}(0)$ describes the recoupling process and would lead to a strong signal decay ($\sim\cos\frac{N}{2}\bar{\Phi}(0)$) under a train of π-pulses. In order to have a measurable effect for the study of intermediate motional effects on the recoupling, an echo is formed by skipping the central pulse in such a train, as shown in Fig. 1a. The total signal is calculated as

$$\begin{aligned} S &= \left\langle \exp\left\{i\frac{N}{2}\bar{\Phi}_1(0)\right\}\exp\left\{-i\frac{N}{2}\bar{\Phi}_2(0)\right\}\right\rangle \\ &= \left\langle \cos\frac{N}{2}\bar{\Phi}_1(0)\cos\frac{N}{2}\bar{\Phi}_2(0) + \sin\frac{N}{2}\bar{\Phi}_1(0)\sin\frac{N}{2}\bar{\Phi}_2(0)\right\rangle \\ &= \left\langle \cos\left(\frac{N}{2}\bar{\Phi}_1(0) - \frac{N}{2}\bar{\Phi}_2(0)\right)\right\rangle. \end{aligned} \quad [4]$$

The angular brackets denote a powder average. Skipping the central π pulse makes the exponential terms in the first line complex conjugates of each other, which corresponds to the echo formation. Assuming that relaxation and other effects leading to a signal decay can be neglected, the general identity of the two phase factors identified with the first and the second half of the recoupled echo ($\bar{\Phi}_1(0) = \bar{\Phi}_2(0)$) implies that no effect of recoupling would be expected for the final intensity. Signal decay due to relaxation and other experimental problems can be corrected for by comparing this signal to that measured after a simple Hahn-echo sequence with delays $\frac{N}{2}\tau_R$, as shown in Fig. 1b. If motions in the intermediate regions have a pronounced effect on the recoupling, this will be evident from a comparison of the signal intensity in these two experiments. As will be shown below, finite pulses in particular introduce further adverse effects which obscure the principal effect on CSA recoupling. Our primary concern is, however, to investigate the main effect of intermediate motions on CSA recoupling independently from other interactions in the spin system.

The principle of recoupling introduced in the preceding discussion can be applied in different ways. One possibility is the measurement of the static (or fast-motion limit averaged) CSA tensor parameters in a 2D experiment, in which the high-resolution ^{13}C dimension under fast MAS (virtually no spinning sidebands) is correlated with an indirect dimension in which the time-modulation described in Eq. [3] can be exploited to generate a special kind of spinning sideband pattern. When a t_1 dimension is inserted into the recoupled echo sequence of Fig. 1a (*18*), the signal becomes

$$S_{RRE} = \left\langle \cos\left(\frac{N}{2}\bar{\Phi}_1(0) - \Phi(0;t_1) - \frac{N}{2}\bar{\Phi}_2(t_1) + \Phi(t_1;2t_1) \right) \right\rangle. \quad [5]$$

The dominant terms in this equation are the $\frac{N}{2}\bar{\Phi}_i(t)$; if MAS is assumed to totally suppress evolution under the CSA during the t_1 evolution periods, the two $\Phi(t_a;t_b)$ terms can be neglected. The dependence upon the tensor parameters δ and η implicit to Eq. [5] can either be exploited directly, as done by Hong (*18*) in an application to CSA determination in peptides, or a cosine Fourier transform can be performed over the time-domain data after a possible catenation and appropriate damping of signal covering one or several rotor periods of t_1 modulation. The sideband pattern thus obtained is special in that it does not map out the spectral range of the recoupled anisotropic interaction, but can be pumped to cover a much wider frequency range. The underlying mechanism was termed *reconversion rotor encoding* (subscript RRE) and is simply due to the γ-dependence of the Hamiltonian during the second recoupling period (Eq. [3]). RRE was first discovered in homonuclear double-quantum experiments (*20–22*), where the two separate recoupling periods are identified with the excitation and reconversion periods for the double-quantum coherence, hence the name. The RRE mechanism was also exploited in similar heteronuclear experiments, in which REDOR recoupling under very fast MAS was used to recouple and precisely measure ^{13}C–^{1}H dipolar coupling constants (*23, 24*). The results reported here for CSA as our model interaction can be generalized to all these classes of experiments. Note that for $\eta = 0$ ($\Rightarrow S_1 = 0$) the angular dependence of the phase given in Eq. [3] is identical to that acquired under BaBa recoupling (*22*) of homonuclear dipolar interactions and under REDOR recoupling (*17*) of heteronuclear dipolar interactions.

A second application of CSA recoupling under MAS is the CODEX (centerband-only detection of exchange) sequence (*7*) for the study of slow tensor reorientations. Figure 1d shows the pulse sequence. The recoupling periods are now separated by a rotor-synchronized mixing time of up to several seconds length, during which the magnetization is stored on $\pm z$ by $\pi/2$-pulses. If reorientation occurs during τ_{mix}, $\bar{\Phi}_2$ of Eq. [4] is no longer equal to $\bar{\Phi}_1$, and consequently a τ_{mix}-dependent signal decay is measured, which depends on the rate of the slow process. In order to obtain results which are corrected for relaxation phenomena, a trick is employed: the experiment is conducted with a second z-filter of duration τ_d (dephasing delay) which is usually quite short (one or several τ_R, just the time needed for the rotor trigger). Interchanging τ_{mix} and τ_d constitutes a reference experiment of equal overall experimental time (equal loss due to T_1 relaxation), in which virtually no exchange occurs between the recoupling periods. By subtracting the intensity which is left after the exchange experiment (E_{ex}) from the reference (E_{ref}), and dividing by E_{ref}, a normalized exchange intensity $E = 1 - E_{ex}/E_{ref}$ is obtained in the limit of long recoupling times, which is only a function of the number of molecular sites M accessible to the dynamic process, $E_\infty = (1 - f_i)(M - 1)/M$, where f_i is a possible fraction of immobile segments. It will be a subject of investigation here if these relations still hold when the rate of the process enters the intermediate motional regime. The concept of using a recoupled interaction for the study of slow dynamics is general in that, using BaBa recoupling of homonuclear dipolar interactions, it has also been shown to be possible to study the reorientation of ^{13}C–^{13}C bonds (*8*).

Intermediate motional regime and numerical simulations. Theoretical approaches to the description of molecular motions on the experimental timescale of a MAS experiment are numerous and have been published on almost every level of sophistication. First attempts were limited to the description of the centerband width in MAS spectra. Waugh and co-workers (*11*) used an approach based on semiclassical relaxation theory as well as on an analytical solution of the stochastic Liouville–von Neumann equation

$$\frac{\partial}{\partial t}\hat{\rho}(t) = \hat{\hat{L}}(t)\hat{\rho}(t), \quad [6]$$

where

$$\hat{\hat{L}}(t) = -i\hat{\hat{H}}(t) - \hat{\hat{K}} \quad [7]$$

is the Liouville superoperator. Relaxation is neglected in these equations. $\hat{\hat{K}}$ is the statistical operator, whose matrix representation is the exchange matrix **K** containing individual rate constants k_i connecting the different sites, and $\hat{\hat{H}}(t)$ is the Hamiltonian superoperator, the time dependence of which is governed by MAS and by the sequence of RF pulses applied to the system. All published solutions of Eq. [6] follow one essential protocol: as a first step, a suitable eigenvalue representation of $\hat{H}$ has to be identified. Equation [6] can be then transformed into the corresponding interaction frame. One is left with a system of coupled differential equations, with a time dependence being determined by the transformed $\hat{\hat{K}}$. However, a solution can only straightforwardly be obtained when one restricts oneself to the eigenvalues of $\hat{\hat{H}}(t)$ in the centerband approximation (*11*). This means that the MAS time dependence of $\hat{\hat{H}}(t)$ is neglected, which clearly limits the applicability of the approach to $k_i < \omega_R/2\pi$.

For a full solution, the appropriate eigenstate representation is constituted by the so-called Floquet states, which represent the individual sidebands; unfortunately, a strict treatment requires considering an infinite number of these states. The corresponding theory has been worked out by Schmidt and Vega (*25*). Some simplifications of this approach, in particular concerning the truncation of the Floquet space to a manageable size, are due to Luz *et al.* (*26*). An even simpler fully analytical approach was published by Frydman and Frydman (*27*), who found that the main features of the spectra could be explained by replacing the time dependence under MAS during one rotor period by only three subsequent evolutions with different appropriately calculated single frequencies.

These analytical approaches are unwieldy when it comes to calculating the spin evolution under a pulse sequence, as is required in our case. Even though we anticipate that suitable models can be derived to tackle the problem analytically, our first approach reported here is based on a time-ordered numerical integration of Eq. [6]. Since the matrix dimensions in Liouville space become exceedingly large upon increasing the number of spins and/or accessible sites of the dynamic process, this brute-force approach is computationally very demanding. Considerable time savings can be accomplished again by transforming into an eigenvalue representation and solving only the exchange part numerically. In such a time-slicing method, the MAS time dependence is straightforwardly included in the calculation by letting the eigenvalues vary with time (*28*). The calculations for our simple model case (CSA tensor reorientation of a single spin) could clearly be most efficiently tackled by this approach. However, sacrificing speed for generality, we chose to modify a homewritten spin dynamics code based on evaluating the finite-step propagator $\exp\{-i\hat{H}(t)\Delta t\}$ in Hilbert (product) space. This program is in many respects very similar to the recently published SIMPSON software (*29*).

The formal solution of Eq. [6] is given by (*30*)

$$\hat{\rho}(t) = \exp\left\{\int_0^t \mathrm{d}t'\,\hat{\hat{L}}(t')\right\}\hat{\rho}(0). \qquad [8]$$

The matrix representation of the Liouville superoperator is constructed as

$$\hat{\hat{L}}(t) = -i\,\mathbf{H}(t)\otimes\mathbb{I} + i\,\mathbb{I}\otimes\mathbf{H}(t) - \mathbf{K}\otimes\mathbf{K}. \qquad [9]$$

Thus, generalizing the finite-step integration concept to the exchange case would in principle require many diagonalizations of very large Liouville-space matrices. The dimension of the Hilbert-space density matrix for N spins and M magnetically inequivalent sites (assuming an equal number of spins per site) is already 2^{N+M-1}, while $\dim(\hat{\hat{L}})$ is even the square of that! We are aware of only one publication where a calculation of this kind has been undertaken for the FID of a four-spin system undergoing a three-site jump (a rotating $-NH_3$ group) evolving under MAS and heteronuclear cw decoupling (*14*). The Liouville matrix in this case is only of dimension $16^2 = 256$, because the 3-site jump can be mimicked by a permutation between the 3 protons ($M = 1$). Also, the authors identified a further block structure in the Liouvillian to make the problem amenable to computer simulations. For a fully general program, it is desirable to retain all components of the density matrix, not only the ones corresponding to, say, single-quantum coherence of one spin, and to be able to include exchange processes connecting geometrically independent sites.

Fortunately, the high-temperature approximation itself includes an immediate reduction of the dimensionality of the problem (*30–32*). In essence, $\hat{\rho}$, which represents a state vector in the $2^{2(N+M-1)}$-dimensional Liouville space, can be considered as an M-component *vector* in a *composite Liouville space* of dimension $M \times 2^{2N}$ (*30*). We write

$$\hat{\boldsymbol{\rho}}(t) = (\hat{\rho}_1(t), \hat{\rho}_2(t), \ldots, \hat{\rho}_M(t)) \qquad [10]$$

for the composite density matrix. $\hat{\rho}_i$ are the density matrices for each of the sites. Finally, restricting ourselves to cases of *intermolecular* exchange (i.e., no spin permutations), the exchange matrix **K** is easily realized to mix only between each of these sites, and not between individual components of $\hat{\rho}_i$. **K** is thus just an M-dimensional *coefficient matrix*, in the same sense as in the cases in which it mixes between magnetization components with individual frequencies in the eigenvalue representation of the problem. Analogously, each site has its own Hamiltonian $\hat{H}_i$, such that the quantum-mechanical part of Eq. [6] leads to mixing only between the components of the associated $\hat{\rho}_i$. Exclusion of intramolecular exchange is not a big restriction, since spin permutations can also be realized by an appropriate number of replica $\hat{\rho}_i$'s with associated $\hat{H}_i$'s in which the the spin

operators are permuted. The extra amount of calculation time scales only linearly with the number of permutations.

While the formal solution of Eq. [6] necessitates a diagonalization of $\hat{\hat{L}}$, the finite-step approach allows us to separate the quantum-mechanical part from the exchange part, the latter of which has just been shown to be interpretable classically. Neglecting exchange, each of the components of $\hat{\underline{\rho}}$ is propagated using the familiar bilinear transformation in Hilbert space,

$$\hat{\rho}_i(t + \Delta t) = \exp\{i\hat{H}_i(t)\Delta t\}\hat{\rho}_i(t)\exp\{-i\hat{H}_i(t)\Delta t\}, \quad [11]$$

while the exchange step is calculated as

$$\hat{\underline{\rho}}(t + \Delta t) = \exp\{-\mathbf{K}\Delta t\}\hat{\underline{\rho}}(t). \quad [12]$$

These two steps are executed sequentially, and a complete cycle represents the true evolution for one Δt. Only one diagonalization of the matrix $\mathbf{K}$ is needed in the whole calculation. As an example, the exchange matrix for our model two-site jump reads

$$\mathbf{K} = \begin{pmatrix} -k & k \\ k & -k \end{pmatrix}, \quad [13]$$

while $\hat{\underline{\rho}}(t)$ has only two components representing the coherences and populations associated with the individual sites.

For best calculation efficiency, a small number l of propagator sets (M individual ones) covering one rotor period, usually $l = 20$–40 depending on the timestep necessary to achieve convergence for the quantum-mechanical part of the evolution, can be prepared at the start of the calculation for each powder orientation. If the rate constants in $\mathbf{K}$ become very high, the timestep $\Delta t = l/\tau_R$ might be too big. In such cases, we still prepare l MAS propagators separated by l/τ_R, but with a new, shorter timestep Δt_{ex}:

$$\hat{U}_i(t) = \exp\{-i\hat{H}_i(t)\Delta t_{ex}\}; \quad t = 0, \frac{1}{\tau_R}, \frac{2}{\tau_R}, \ldots, \frac{l-1}{\tau_R}. \quad [14]$$

Equations [11] and [12] are then still applied in turns using the shorter Δt_{ex}, but with a constant MAS propagator for each sequence of $\Delta t/\Delta t_{ex}$ steps. In this way, a whole pulse sequence can be calculated without any diagonalizations during the spin evolution calculation. The calculation time is thus mainly determined by the speed at which matrix multiplications can be performed. Moreover, if finite RF pulses are to be included, l additional propagator sets must be prepared for each irradiation pattern at a given time. Our program is so far limited to δ-pulses, which are simple spin space rotations, the propagators for which are calculated before entering the sequence calculation anyways.

The separation of the quantum-mechanical and the exchange part of the time evolution has another very beneficial implication: when an exchange experiment is to be simulated, where the magnetization is stored on $\pm$z during a comparatively long mixing time, the exchange process can be simulated by omitting the quantum-mechanical part of the evolution calculation. This is strictly correct only when the interaction Hamiltonian commutes with $\hat{I}_z$ (e.g., no spin diffusion), but this condition should hold for most of the scenarios of interest. The remaining evolution due to exchange need moreover not be simulated in small steps of Δt_{ex}; rather, the exponential of the exchange matrix, $\exp\{-\mathbf{K}\Delta t_{mix}\}$, can be calculated by just one diagonalization of $\mathbf{K}\Delta t_{mix}$. The ensuing propagation of $\hat{\underline{\rho}}$ is then performed in a single step. Slow exchange phenomena over very long times can thus be simulated with virtually no increase in the overall calculation time.

3. EXPERIMENTAL

Simulations. The validity of the algorithm presented above was checked by repeating several simulations detailed in the references given in the above theory section. In all cases, our results matched the ones from the references as close as it was possible to gauge by visual inspection. The timestep Δt was 2 μs in all cases, while using a shorter Δt_{ex} (down to 0.2 μs) was beneficial only for the sideband pattern calculations in Section 4.2, first part, where the fast-limit case was reached.

Pulse sequences. Pulse sequences as schematically shown in Fig. 1 were used for all experiments. For simplicity, ^{1}H preparation and CP pulses as well as decoupling periods were omitted in the figure. Decoupling was applied during the whole course of the sequences, with the exception of the CODEX sequence in Fig. 1d, where it is omitted during τ_{mix} and τ_d. τ_{mix} contains a rotor trigger, which is timed relative to a trigger at the start of the pulse sequence, to ensure the same inital rotor phase at the start of both recoupling periods. For the CSA sideband spectra, incrementable t_1 evolution periods were added to the sequence in Fig. 1a. In addition, a z-filter is appended to ensure an amplitude-modulated signal in t_1, and hence pure absorption-mode lineshapes in the 2D frequency-domain spectrum.

The phase cycles were the same as those conventionally used in CP experiments, i.e., eight-step cycles comprising spin temperature inversion of the ^{1}H preparation pulse and CYCLOPS of the ^{13}C CP pulse for quadrature artifact suppression. Pulse imperfections in the π-pulse trains were reduced by applying xy-4 phase cycling (*33*). An additional two-step cycle was added for sequences with z-filters in order to better suppress transverse signals surviving these. This is particularly important for DMS, which has a rather long T_2 even without decoupling. For the CODEX experiment, we implemented a new and improved phase cycle (*34*), which was developed for this purpose.

While the reference experiment for the recoupled echo (Fig. 1b) as proposed above is successful in serving as a normalization for intensity loss which is associated with reorientations

of the nonrecoupled CSA tensor, it does not account for other adverse effects. Although the xy-4 phase cycling removes most problems associated with the π pulse trains, imperfections are still responsible for some signal loss. Moreover, heteronuclear recoupling effects due to interference of finite pulses with the decoupling field can be very large (*35*). In order to avoid such effects, the decoupling field should be three times higher than the field associated with the recoupling pulses. This condition is hard to meet when a further requirement is that recoupling pulses should be as short as possible in order to obtain results which can be described by theory using the δ-pulse approximation (in our case 2 μs for the 2.5-mm probehead). Therefore, we used a reference experiment which has virtually the same duty cycle as the recoupled echo (Fig. 1c), but does not exhibit CSA recoupling to a first approximation. This is achieved by moving the π-pulses located in the middle of each τ_R in the recoupling sequence towards the end of the same rotor cycle, thus forming pairs of π-pulses. Using a crystalline substance without intermediate motions of ^{13}C (L-alanine), we checked the equality of the recoupled and the reference echo. Simulations confirmed that, considering only CSA reorientations, intermediate motional effects on a single Hahn echo and on the reference echo with many pulses and τ_R spacings are identical.

Note that in the light of the large effects introduced by the finite pulses to be reported below, it is a rather complex task to find a reference pulse sequence which also compensates the contribution from the interference of intermediate motions and such higher-order effects. The reference experiment reported here represents a first, pragmatic approach towards studying the CSA effect in an isolated fashion. Truly quantitative results might only be expected from an inclusion of such effects into the simulations, which is outside the scope of this paper, or from the use of hardware which allows the application of considerably higher pulse power levels.

NMR experiments. All experiments were performed on a Bruker Avance 500 solid-state NMR spectrometer, equipped with an 11.7-T wide-bore UltraShield^{TM} magnet, and running at Larmor frequencies of 500.2 and 125.8 MHz for protons and carbons, respectively. The recoupled echo measurements were performed using a 2.5-mm MAS probe with typical $\omega_1/2\pi$ frequencies of 125 kHz for ^{13}C and ^{1}H pulses, and 125 kHz for TPPM decoupling (*36*). Decoupling during the π pulse trains was increased to 156 kHz. The sideband and CODEX applications were measured with a 4-mm MAS WVT probe. Typical power levels corresponded to 62.5 kHz for pulses and ^{1}H decoupling during acquisition, and 83.3 kHz for decoupling during the pulse trains. In both cases, cross polarization was achieved using a ramp (*37*) with typically 1024 steps applied to the proton channel ranging from 80 to 100%. The carbon spin lock was centered on the sideband match condition $\omega_{1,C} = \omega_{1,H} - \omega_R$, with $\omega_{1,H}$ corresponding to the 90% level of the ramp. These power levels were decreased by about 30% relative to the single-pulse powers given above.

An important issue is the temperature calibration of MAS NMR probes. Considerable cooling (Joule–Thomson) and heating (bearing friction) effects occur particularly at fast spinning (*38, 39*). Both bearing and drive pressures, as well as the resulting spinning frequency, influence the sample temperature, T_s. Using $Sm_2Sn_2O_7$ as a chemical-shift thermometer, we fitted T_s, as obtained from the isotropic ^{119}Sn shift by numerically solving the $T_s - \delta$ relation given in (*40*), to the equation

$$T_s = a_0 + a_1 T_b + a_2 \nu_R + a_3 \nu_R T_b + a_4 \nu_R^2 + a_5 \nu_R^2 T_b + a_6 T_b^2. \quad [15]$$

The last two terms were not necessary for a good fit in Refs. (*38, 39*) (a_6 was only significant for our 4-mm probe). Presumably, they are only important when very large temperature ranges are covered. The effect of drive and bearing pressure is included in ν_R, where care must be taken to have reproducible pressures for a given ν_R. Also, the mode of measuring the temperature, T_b, is important. Our probes are equipped with separate PT100's measuring the bearing or VT gas temperature before it reaches the rotor, and when it leaves the stator. These temperatures can be different by more than 10 K! Reproducible results for equilibration times of approximately 5 minutes after temperature changes of 10 K were obtained by calibrating at the output and the input of our 2.5- and 4-mm MAS probes, respectively (our 2.5-mm probe has a separate input for VT air). A different setup necessitates much longer equilibration times (more than 20 minutes). We do not give the fitting parameters a_i here since they are probe dependent and must be determined for every individual probe. Temperature gradients in a full rotor can be severe in particular for 2.5-mm MAS probes. We measured gradients of 4–6 K at the high (340 K) and low (250 K) temperatures at 30 kHz MAS. The gradients under the experimental conditions used in this paper are not bigger than 1.5 K.

Sample. Dimethyl sulfone ($(CH_3)_2SO_2$, DMS) was purchased from Aldrich and used without further purification. The chemical-shift parameters for the CH_3-group were taken from Ref. (*15*): $\delta/2\pi = 37.3$ ppm, $\eta \approx 0$. The unique principal axis of this symmetric tensor reorients by $\beta = 108^\circ$ as a result of a two-site exchange process, which is more easily visualized as a 180° jump of the molecule around an axis through the S atom, bisecting the C–S–C angle. The theoretical rate constants were calculated from the Arrhenius equation

$$k_{th} = k_0 e^{-E_a/RT}; \qquad k_0 = 4 \times 10^{16}\,\mathrm{s}^{-1}, \qquad E_a = 83\,\mathrm{kJ/mol}. \quad [16]$$

The activation parameters were published in (*16*). This paper contains a combination of new measurements and a wealth of literature data on NMR-determined rate constants for DMS. To our knowledge, it is the most reliable database for the Arrhenius fit.

4. RESULTS AND DISCUSSION

DMS is a convenient model system for studying the intermediate motional regime (as seen relative to its ^{13}C tensor width, $\delta/2\pi = 4.7$ kHz at 125.8 MHz) since its correlation time spans the whole region from the slow limit at around 0°C ($k_{th} =$ 5 Hz) to the fast limit right below its melting point of 108°C ($k_{th} = 170$ kHz). First, we present simulations using the parameters for DMS in order to highlight the main effect of intermediate motions on recoupling and then prove our findings experimentally. Second, we show how this knowledge helps us in understanding actual applications of recoupling techniques.

It should be again emphasized that the main concern of this paper is to gain a first understanding of the effect of intermediate motions on the recoupling of a single interaction. In order to demonstrate this, we show simulations in which CSA is the only interaction being taken into account. As will become apparent from the experimental data, adverse effects which are introduced by experimental imperfections (finite pulses) and are mediated by other interactions (homo- and heteronuclear dipolar couplings) contribute to the signal. Consequentially, we attempted to isolate the CSA effect experimentally by using a reference experiment.

4.1. The Effect of Recoupling

Simulations. Figure 2 presents results from simulations of the intensity of a recoupled echo (Fig. 1a) and the reference echo (Fig. 1b or 1c) for three different spinning speeds. The intensities are represented as 2D surface plots as a function of

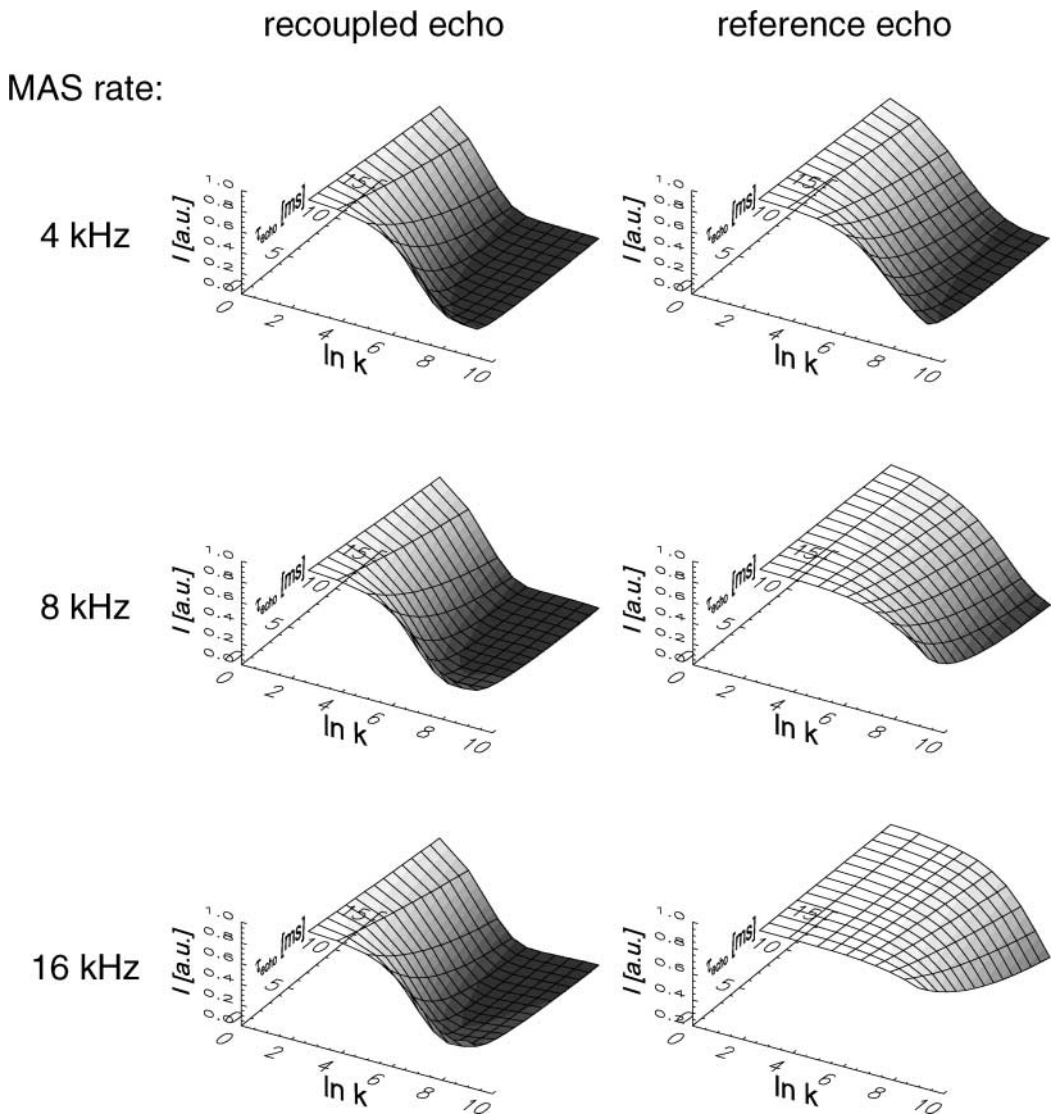

FIG. 2. Intensities for the recoupled echo (Fig. 1a) and reference echo (Fig. 1b or 1c) experiments, as obtained from simulations using the methyl ^{13}C CSA tensor parameters for the two-site jump in DMS, as a function of the correlation rate, k, and the total echo delay, τ_{echo}.

the correlation rate k and the echo delay (in ms). Note that the jump rates cover only the region where $k \leq \delta$. As a general trend, the intensity is seen to decrease with increasing echo delay and increasing k, as the intermediate motional regime is entered. As is also to be expected, the decay of the reference echo is lessened when spinning at higher frequencies, since at very high ν_R, the anisotropic interaction, whose angular fluctuations lead to signal loss, is simply averaged out.

Most importantly, however, the signal loss of the *recoupled* echo is hardly dependent at all on the spinning frequency. Conceptually, this observation is very attractive in that ω_R should not appear as a parameter in a theoretical model describing this decay. An analytical description of the phenomenon is not yet available, but the simulations show that it is apparently the average *recoupled* tensor, as described by Eq. [3], whose fluctuations govern the decay.

In the following, we will use the ratio of the recoupled to the reference echo intensities as an experimentally accessible entity, and analyze its dependence on k more quantitatively. As far as the ensuing comparison with experimental data is concerned, it must be remembered that signal loss during NMR experiments occurs as a result of various factors, such as the interference of heteronuclear decoupling and motions of the C–H dipolar tensor (*12, 14*), or recoupling effects of finite pulses (*35*). Such effects are *not* included in the simulations. However, if the reference experiment meets the requirement of being subject to the same adverse effects, the ratio I_{rcpl}/I_{ref} should reflect only the effects of intermediate motions on the recoupling. Figure 3 shows the decay of this ratio for different rates, simulated at 16 kHz MAS. If a quantitative study along these lines is intended, fast spinning with $\omega_R \gg \delta$ is very important in order to retain as much signal as possible for the reference experiment, as the final error margins sensitively depend on this. The general conclusions to be drawn from our analysis will thus only be valid for this regime.

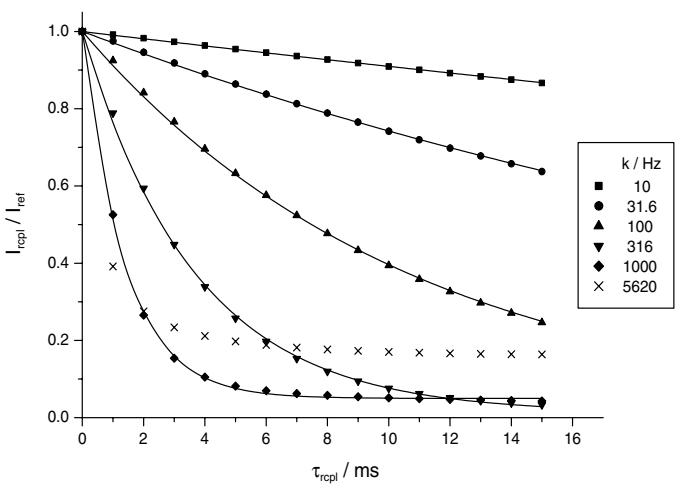

FIG. 3. The intensity of the recoupled-echo experiment divided by that of the reference-echo experiment as a function of the motional rate, k, of the jump process in DMS, as obtained from simulations for 16 kHz MAS. The lines correspond to fits to the simulated points using single exponential decay functions. For the fit of the data at $k = 1000$ Hz only, an offset from the zero level for $\tau_{rcpl} \to \infty$ has been included in the fit.

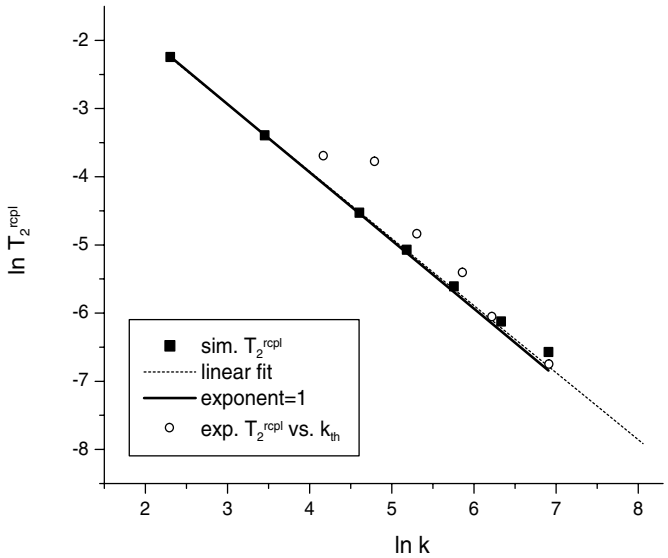

FIG. 4. T_2^{rcpl}, as determined from fits of the simulated data in Fig. 3 to single exponential functions (■), plotted versus the rate constant of DMS, k. The dashed line is a linear fit to the first five points in ln–ln representation, the thick solid line has a slope of -1. Experimental values (see Fig. 5) are shown as open circles (○).

The data in Fig. 3 can be well-fit to single exponential functions, the decay time constants of which (T_2^{rcpl}) decrease with increasing k. Only when the rate approaches $k \approx \delta/2\pi$ does I_{rcpl}/I_{ref} decay to a finite value, and the data no longer fit to a simple exponential. This is indicative of what happens when the fast limit, $k \gg \delta$, is approached. In this case, recoupling will not be influenced by the motion any more, the echo formation is well behaved again and follows Eq. [4], with phase factors depending on the dynamically averaged tensor. Figure 4 depicts T_2^{rcpl} vs k in a ln–ln plot. A straight line represents a very good representation of the functional dependence. Fitting of the first five points ($k = 1$–$316\,\mathrm{s}^{-1}$) yields

$$\ln T_2^{rcpl} = 0.013 - 0.984 \ln k. \qquad [17]$$

Thus, the relationship can be approximated well by

$$T_2^{rcpl} = 1.01/k. \qquad [18]$$

The proportionality factor is close to one by mere chance and is dependent on δ and the geometry of the process, as further simulations indicated.

Experimental confirmation. Recoupled and reference echo experiments, as explained under Pulse sequences, were performed on DMS at different temperatures and a spinning frequency of 16 kHz. Even though the simulations suggest that the

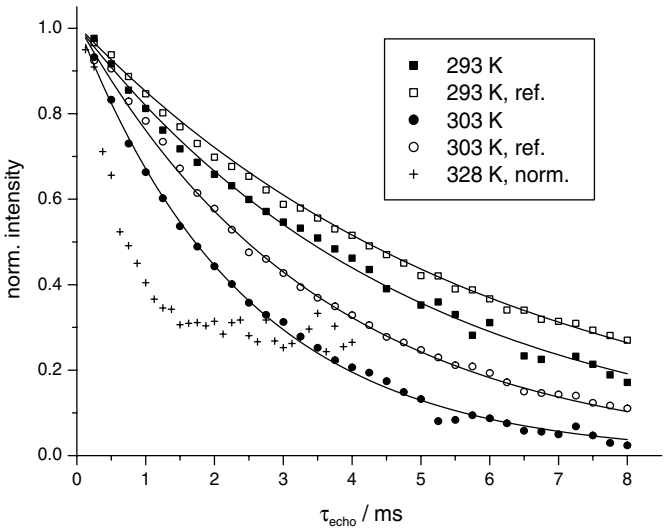

FIG. 5. Raw data from recoupled (solid symbols) and reference (open symbols) echo experiments performed on DMS at different temperatures with $\omega_R/2\pi = 16$ kHz. The solid lines are fits using a single exponential decay function. The crosses represent already normalized data, I_{rcpl}/I_{ref}, for illustration of the intensity plateau, which is reached upon entering the fast limit. In this limit, the exponential decay approximation breaks down.

reference echo should decay only very slowly under these conditions, the data in Fig. 5 indicate that this is not the case. In fact, in particular at lower temperatures, the decay of the reference echo is only slightly slower than the decay of the recoupled echo. Adverse effects such as the interference of finite π pulses or dynamics with the heteronuclear decoupling are therefore large. Note that a similarly strong decay was observed for the methyl group of L-alanine, where in the absence of motion the large loss of spectral intensity with increasing recoupling time was almost identical for recoupled and reference echo, proving the validity of the reference experiment.

Reliable results could be extracted from the data by fitting the individual decays and calculating T_2^{rcpl} as $1/((T_2^{rcpl,exp})^{-1} - (T_2^{ref})^{-1})$. The data thus calculated are plotted in comparison with the results from simulations in Fig. 4 (open circles), where the rate constant, k_{th}, was determined from the sample temperature by use of Eq. [16]. The agreement of the experiments and the simulations is good, confirming the effect of intermediate motions on recoupling as discussed above. Deviations occur in particular for lower temperatures, where a larger error due to the small difference of $T_2^{rcpl,exp}$ and T_2^{ref} must be expected. We would expect that better results could be obtained from substances with reorienting quaternary carbon atoms, where the decoupling problem is less serious and the referencing procedure is less critical.

The above analysis is limited to $k \leq \delta/2\pi$. The crosses in Fig. 5 show the decay of the recoupled echo at $T = 328$ K (corresponding to $k_{th} = 2.42$ kHz), which is already normalized by $e^{+t/T_2^{ref}}$. The data confirm the existence of an intensity plateau when the process becomes fast on the experimental timescale. For increasingly large k, the recoupled tensor is the fast-limit averaged tensor, and the motion will not effect the recoupling process any more. The measurement of tensor parameters over the whole range from the slow to the fast limit is the subject of the next section.

4.2. Applications

As we were primarily concerned with illustrating the effect of the onset of intermediate motions on the recoupling using computer simulations and idealized experiments, we will now focus on pulse sequences which are used in practical applications. These results will be serve as examples for the limits and possibilities posed by the interplay of recoupling and dynamics in general. The methods used here were explained in Section 2.

Influence on tensor parameter measurements: CSA sidebands. A comparison of experimental and simulated recoupled CSA sideband patterns is shown in Fig. 6. Equation [5] describes the t_1 time domain signal of an incremented recoupled-echo sequence (Fig. 1a), which has been Fourier-transformed to give the sideband spectra. Upon passing through the intermediate motional regime ($k \approx \delta/2\pi$), a clear transition from spectra dominated by about 4 sideband orders to spectra dominated by 2 sideband orders can be observed. Notably, spectra different from the limiting

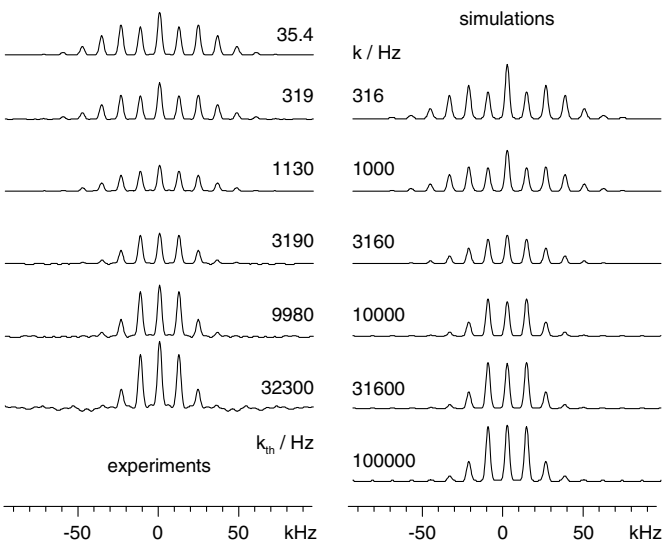

FIG. 6. Spinning sideband patterns, as obtained by rotor encoding of the CSA tensor of DMS using the pulse sequence in Fig. 1a. For each spectrum, 2 rotor periods of t_1 evolution (32 individual spectra) were measured, extended 10 times, and zero-filled to 512 points prior to Gaussian apodization (3 kHz) and a cosine Fourier transformation. The experiments were performed using a 4-mm MAS system with a spinning frequency of 12 kHz and a constant overall recoupling time of 8 τ_R ($N = 8$) at different temperatures. The rate constants, k_{th}, were calculated from Eq. [16]. The corresponding patterns on the right hand side are full computer simulations of the pulse sequence, as described under Theoretical Background. The integral intensities within each of the columns are to scale; see the caption of Fig. 7 for details.

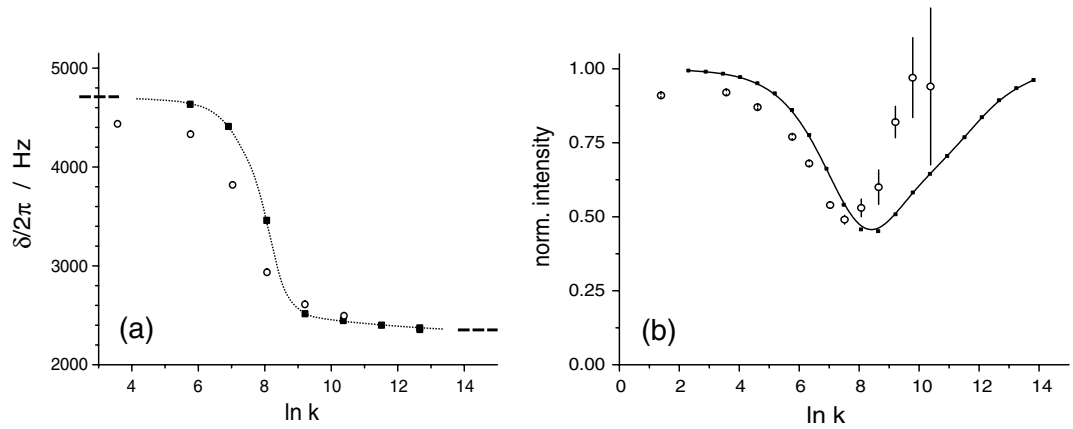

FIG. 7. Anisotropy parameters, δ, as obtained from fitting the sideband spectra in Fig. 6a; and integral intensities of the sideband patterns (b). In (a), the limiting values for δ are denoted by thick dashed lines. In (b), the absolute intensities were determined by comparing the intensity of the first slices ($t_1 = 0$) of the 2D spectra with regular cross-polarization spectra. The latter featured a Hahn echo and a final z-filter, the lengths of which were matched to the equivalent delay times of the CSA recoupling sequence. The data in (b) were supplemented with intensities of individual $t_1 = 0$ slices at different temperatures. Open circles (○) are experimental points; solid squares (■) are from computer simulations. Dotted lines are guides to the eye.

cases are only seen in a very narrow interval where $k \approx \delta/2\pi$. This is also the region where the integral intensity of the spectra is at a minimum.

Before discussing the intensity issue in more detail, we turn to a quantitative determination of the tensor parameters. Both the experimental and the simulated spectra were numerically fitted to spectra calculated from Eq. [5] using a computer program comprising the Levenberg–Marquardt least-squares fitting algorithm (*41*) and a numerical calculation of the derivatives of powder-averaged spectra with respect to the fitting parameters. In theory, the CSA tensor of DMS is symmetric ($\eta = 0$) in the static limit, with $\delta/2\pi = 4.7$ kHz, and almost perfectly asymmetric ($\eta = 0.996$) with $\delta/2\pi = 2.3$ kHz in the case of rapid averaging over the two positions. These limiting cases are indeed found, as shown in Fig. 7a. Fitting the simulated patterns, the best-fit (lowest χ^2) always yielded an η close to 0 for $k < 5$ kHz, and $\eta \approx 1$ for larger k, confirming that the patterns closely resemble the limiting cases over very wide ranges of rates.

Our experimentally determined δ in the static limit is slightly smaller (4.4 kHz) as compared to the literature value. One possible complication is the instability of the fit with respect to the simultaneous fitting of δ and η. While fitting η to simulated spectra including intermediate motions is still possible with good accuracy, slight experimental errors can hamper the determination of η. The asymmetry is not very sensitively encoded in the sideband patterns, and it is known that the method is generally not well suited for its determination (*18*). However, in a separate study (*42*) it was found that δ is always accurate within about 10% even when η is not known. The best-fit η to the experimental patterns varied from 0.3 to about 0.5. Comparing the experimental and simulated values of δ in Fig. 7a, a shift over approximately a quarter decade in k is apparent. This shift might be attributed to a temperature calibration problem—1/4 decade in k corresponds to about 5 K. Even though we took good care to perform the experiments under the same conditions as the temperature calibration measurements, it cannot be excluded that variations in drive and bearing pressures, which occur using rotors of different quality and filling, are a part of the problem, especially at fast MAS (12 kHz).

The shift of experimental vs simulated data in k is also observed for the integral intensities of the sideband patterns (Fig. 7b). This plot is only to be interpreted as a general trend, since the determination of absolute intensities for experiments conducted at different temperatures is an experimentally challenging task. Our normalization is to be taken as a very crude one—the intensity of the first slice of the 2D data was compared with a simple CP sequence followed by a Hahn echo and a z-filter. Nevertheless, the intensity is found to pass through a minimum at approximately $k \approx \delta/2\pi$. The much bigger effect is a general loss of overall signal at high T, as reflected in the error bars. The main influencing factor is the interference of the dynamics of the CH dipolar coupling tensors and the cw decoupling (*12*), which leads to serious line broadening (as was observed in the direct dimension), and consequently to substantial relaxation under a long pulse sequence. Despite all the complications, the position of the intensity minimum represents a good estimate of the rate constant at that temperature.

Influence on rate constant measurements: CODEX. At around ambient temperature, the jump process in DMS in still slow enough to be studied with conventional exchange techniques, in which a mixing time is inserted between free evolution periods. During these evolution periods, the transverse coherence acquires a phase factor which encodes the CSA tensor orientation (or other interactions subject to change upon exchange, such as isotropic shifts or dipolar couplings). In the last few years, a variety of 1D MAS exchange methods have been

developed (*43–45*), the latest of which, CODEX (*6*), is very attractive in that it can be applied at very fast MAS (*34*), because the essential information is extracted from the centerband intensity only. This is possible because the CSA tensor information is encoded via recoupling, as explained in the theory section.

Increasingly fast dynamics is expected to interfere with the principle of measurement in CODEX in different ways. First, since the mixing time for the reference experiment cannot be arbitrarily short (at least one or a few rotor periods), it can be expected that if appreciable exchange occurs during this reference period, the expected plateau value of the absolute exchange intensity (E_∞) decreases. Usually, it depends only on the fraction of immobile segments and the number of sites accessible to the process; for the two-site exchange process in DMS, a value of 0.5 is to be expected.

When performing CODEX measurements on DMS, we indeed found a decrease of the plateau value. In order to eliminate the effect of exchange during the finite reference mixing period, we changed the basic experimental protocol: when dealing with very fast motions, the mixing times needed to reach the equilibrium (detailed balance) are short enough for the optical rotor trigger to be suspended in favor of a perfectly timed mixing period ($N\tau_R$). The minimum τ_{mix} is then just 1 τ_R (83 μs at 12 kHz MAS). The final dephasing delay for the first experiment is then chosen at least as long as the longest mixing time, and a series of constant-time spectra can be performed by gradually increasing τ_{mix} while at the same time decreasing τ_d. From this series, the correlation time as well as the reference intensity for $\tau_{mix} = 0$ can easily be determined by exponential fitting. The absolute value for the intensity plateau is then obtained in the usual way as $E(\tau_{mix} \to \infty)/E(\tau_{mix} = 0)$.

Results from CODEX experiments at four different temperatures are shown in Fig. 8. With the exception of the lowest temperature, where k was low enough to use the trigger without a sacrifice in accuracy, the mixing time was incremented in full rotor periods as described above. In all cases, the rate constants could reliably be fitted, as can be seen in Table 1, where the experimentally determined rate constants are compared with the ones calculated from the temperature dependence (Eq. [16]). The agreement is very good. However, the plateau values are still found to be much decreased at higher temperatures. Since the extrapolation to $\tau_{mix} = 0$ was used, finite mixing time effects can be excluded.

In order to confirm that intermediate motional effects on recoupling are responsible for this effect, we performed computer simulations of the full CODEX sequence including the mixing time. Again, the calculations were performed for a single spin exhibiting CSA. The time-saving aspects when dealing with calculations of comparatively long mixing times were explained in the theory section. Using the correlation rates as determined from the fits, we obtained the thick grey curves in Fig. 8. These decay with exactly the right rate constant and show the characteristic decay of the plateau (see Table 1). Note

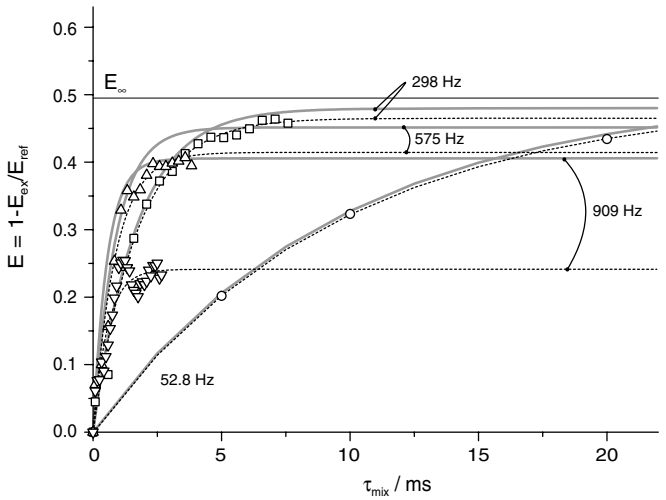

FIG. 8. CODEX absolute exchange intensities, E, measured on DMS at 12-kHz MAS and $10\tau_R$ total recoupling time. Dashed lines represent exponential fits to the data, which yielded the indicated rate constants ($k_{exp} = 1/2\tau_c$). These constants served as a basis for full computer simulations of the CODEX exchange signal, which are shown as thick grey lines. Table 1 gives a comparison of the experimental rate constants and plateau values with those calculated from the sample temperature.

that the calculated plateau value for the experiment at 288 K is slightly bigger than 0.5 because of the finite recoupling time ($\tau_{rcpl} = 10\,\tau_R$ rather than ∞), where the signal oscillates slightly around 0.5.

Most notably, the simulations underestimate the decrease of E_∞ grossly. We must therefore conclude that further effects of motions, such as their interference with effects involving finite pulses and cw decoupling, have a considerable influence. This was somewhat unexpected, since such effects should be the same for any mixing time. For an interpretation, let us first consider the intermediate motional effects on the recoupling which were reproduced in the simulations.

The principle of CODEX depends on a loss of correlation between the tensor orientations during the first and the second recoupling period. These are represented by the phase factors $\bar{\Phi}_1(0)$ and $\bar{\Phi}_2(0)$ in Eq. [4]. In the slow limit, correlation loss

TABLE 1

Comparison of Calculated and Measured Rate Constants ($k_{exp} = 1/2\tau_c$) and Intensity Plateau Values for DMS, as Determined from the CODEX Data (Fig. 8)

T/K	$k_{th}{}^a$/Hz	$k_{exp}{}^b$/Hz	E_∞ (exp.)	E_∞ (sim.)
288	35.4 ± 4.3	52.8 ± 0.50	0.495	0.502
307.5	319 ± 34	298 ± 22	0.465	0.480
313	564 ± 57	575 ± 64	0.415	0.451
320	1130 ± 110	909 ± 136	0.241	0.406

Note. The error due to temperature calibration is estimated to be ± 1 K.

[a] Calculated from Eq. [16].

[b] Errors margins are based on the fit quality.

occurs only as a result of jumps during a long mixing time. When the correlation diminishes additionally due to motions during the recoupling periods, the residual correlation loss, as measured by comparing experiments with long and vanishing τ_{mix}, no longer corresponds to the full amplitude—and the plateau, which measures the amplitude of the correlation loss during τ_{mix} only, decreases.

Coming back to the unexpectedly low plateaus in the experiments, we must conclude that the interference effects between the motion and the decoupling (as mediated by dipolar couplings, not the CSA), contributes to the CODEX signal in a coherent fashion; i.e., there must be a correlation of the CSA-mediated relaxation due to motion and similar effects involving the heteronuclear dipolar coupling tensors. Terao and coworkers (*35*) have indeed identified a coherent higher-order recoupling effect of heteronuclear dipolar couplings due finite π pulses applied to a static sample under conditions of cw decoupling. Similar effects can be expected to be present in the case of the REDOR-type recoupling of ^{13}C CSA in CODEX.

In summary, we have shown that even though CODEX is robust enough to be used to measure fast rate constants in a region approaching the intermediate motional regime, the plateau intensities become rather ill-defined and should not be used for a quantitative evaluation. The argument can, however, be turned around by stating that a decrease of the plateau value at higher temperatures is indicative of intermediate motions. Such an observation might serve as a *qualitative* indication of correlation time distributions in complex systems.

5. CONCLUSIONS

As far as methodological aspects are concerned, an approach towards more efficient numerical simulation of the spin evolution under complicated pulse sequences including molecular dynamics has been presented. In essence, the calculation of the normal quantum-mechanical evolution and the exchange can be separated and carried out sequentially, if only the simulation time step is sufficiently short. The approach is based on a linearization of the Liouville space representation of the problem, which is possible on account of the high-temperature approximation. Therefore, the dimensions of the involved matrices can be much reduced. The cost of the calculation increases only linearly with the number of different sites accessible to the dynamic process. An implementation of this approach into existing spin dynamics codes such as SIMPSON (*29*) is straightforward.

Using simulations and experiments, it was shown that recoupling of a specific interaction (here, the CSA as an example) leads to signal loss when angular reorientations of the recoupled interaction enter the intermediate region. This observation is important for any kind of recoupling in general: in real systems, where many different interactions (CSA, homo-, and heteronuclear dipolar couplings) are present, fast spinning at the magic angle removes the influence of such motions, while recoupling selectively reintroduces not only the desired interaction, but also amplifies the sensitivity of the experiment to angular motions of the associated tensor.

We found a very simple inverse relationship between the rate constant of the process and the apparent relaxation time, T_2^{rcpl}, under the recoupling sequence. The apparent independence of the recoupling-induced decay on the MAS frequency, as seen in the simulations, suggests that the correlation loss between the phases attributed to the *average recoupled tensor* ($\bar{\Phi}_i$ in Eq. [4]), which do not depend on ω_R, is the dominating effect at least in the slow branch of the intermediate motional regime. A theoretical analysis of this model picture in terms of classical relaxation theory is currently underway.

When dealing with applications of recoupling methods on systems with well-defined intermediate motions, we have shown that the apparent transverse relaxation effect and its effect on the integral intensity of the spectra can be used to estimate rate constants, in particular when the intensity minimum, which occurs when k is approximately equal to the interaction parameter in Hz, can be identified. We have further shown that the experiment used to calibrate the absolute spectral intensity has to be chosen carefully and that effects introduced by finite pulses can be large and must ideally be identical in the recoupled and the reference experiment. Generally, recoupling pulses should be as short as possible, and the use of weakly heteronuclear-coupled quaternary carbon atoms as dynamic probes is more promising than the methyl case reported here.

The problem of finite pulses is actually much alleviated for applications in weakly coupled mobile systems, since the MAS frequency and thus the duty cycle can be decreased correspondingly. Therefore, with regards to the application of ^{1}H double-quantum recoupling techniques for the determination of weak residual dipolar coupling constants in mobile systems exhibiting a large number of coexisting timescales such as polymers (*9*), the strong dependence of the signal decay on the size of the fast-limit preaveraged interaction independent of the MAS frequency shown here represents a first step towards interpreting the full ^{1}H double-quantum build-up and decay in terms of intermediate timescales of polymer dynamics. Work along these lines is currently underway in our lab.

Our findings indicate further that popular recoupling methods such as REDOR, which rely on measuring and fitting absolute intensities as obtained through referencing, most likely yield erroneous results when the measured interaction tensor undergoes molecular motions on the timescale of the recoupling. For REDOR in particular, recoupling π pulses are usually omitted (!) on the nonobserve channel for the reference experiment. The large discrepancy between effects of motions on recoupled versus free evolution has convincingly been demonstrated herein. We have recently presented a way of performing the REDOR reference intensity measurement, during which recoupling is still active (*24*), and which should therefore correct not only for homonuclear dephasing effects (which was the subject in that paper), but also for motionally induced signal decay.

Although the spectral intensity is much affected over a very wide range of rate constants under recoupling, the direct measurement of tensor parameters, as achieved by monitoring the rotor-encoding of the interaction tensor in terms of sideband pattern analysis, is still possible with very good accuracy. Such methods are therefore to be preferred over intensity-based approaches. Unfortunately, only a small part of the large number of the many powerful recoupling techniques described in the literature has the desirable amplitude-dependence (as opposed to phase-dependence) of the average Hamiltonian on the rotor position. Examples are REDOR, applicable to CSA and heteronuclear dipolar recoupling (for sideband-pattern based REDOR implementations see (*23, 24*)), and BaBa or DRAMA (*46*) for homonuclear dipolar recoupling.

Finally, it was demonstrated that CODEX, a 1D exchange technique using recoupling, can still be applied for the determination of rate constants in the vicinity of the intermediate motional regime. Even though the method is compensated for most adverse effects under normal conditions, the analysis of the plateau values of the exchange intensity in terms of motional sites and immobile segments is not possible any more.

ACKNOWLEDGMENTS

This work has benefited much from discussions with a large number of colleagues. In particular, we thank K. Schmidt-Rohr, M. Hong, and H. W. Spiess. We acknowledge also C. Schmidt and H. Finkelmann for providing a very productive working environment, S. P. Brown for carefully proofreading the manuscript, and the Deutsche Forschungsgemeinschaft, SFB 428, as well as the Fonds der Chemischen Industrie for financial support.

REFERENCES

1. S. P. Brown and H. W. Spiess, Advanced solid-state NMR methods for the elucidation of structure and dynamics of molecular, macromolecular, and supramolecular systems, *Chem. Rev.* **101,** 4125–4155 (2001).
2. M. Carravetta, M. Edén, X. Zhao, A. Brinkmann, and M. H. Levitt, Symmetry principles for the design of radiofrequency pulse sequences in the nuclear magnetic resonance of rotating solids, *Chem. Phys. Lett.* **321,** 205–215 (2000).
3. A. E. Bennett, R. G. Griffin, and S. Vega, Recoupling of homo- and heteronuclear dipolar interactions in rotating solids, *in* "NMR Basic Principles and Progress" (P. Diehl, E. Fluck, H. Günter, R. Kosfeld, and J. Seelig, Eds.), Vol. 33, pp. 1–77, Springer-Verlag, Berlin (1994).
4. S. Dusold and A. Sebald, Dipolar recoupling under magic-angle spinning conditions, *Annu. Rep. NMR Spectr.* **41,** 185–262 (2000).
5. A. Fechtenkötter, K. Saalwächter, M. A. Harbison, K. Müllen, and H. W. Spiess, Highly ordered columnar structures from hexa-*peri*-hexabenzocoronenes—Synthesis, X-ray diffraction, and solid-state heteronuclear multiple-quantum NMR investigations, *Angew. Chem. Int. Ed. Engl.* **38,** 3039–3042 (1999).
6. E. R. deAzevedo, W.-G. Hu, T. J. Bonagamba, and K. Schmidt-Rohr, Centerband-only detection of exchange: Efficient analysis of dynamics in solids by NMR, *J. Am. Chem. Soc.* **121,** 8411–8412 (1999).
7. E. R. deAzevedo, W.-G. Hu, T. J. Bonagamba, and K. Schmidt-Rohr, Principles of centerband-only detection of exchange in solid-state nuclear magnetic resonance, and extension to four-time centerband-only detection of exchange, *J. Chem. Phys.* **112,** 8988–9001 (2000).
8. I. Schnell, A. Watts, and H. W. Spiess, Double-quantum MAS exchange NMR spectroscopy: Dipolar-coupled spin pairs as probes for slow molecular dynamics, *J. Magn. Reson.* **149,** 90–102 (2001).
9. R. Graf, A. Heuer, and H. W. Spiess, Chain-order effects in polymer melts probed by ^{1}H double-quantum NMR spectrocopy, *Phys. Rev. Lett.* **80,** 5738–5741 (1998).
10. T. Dollase, R. Graf, A. Heuer, and H. W. Spiess, Local order and chain dynamics in molten polymer-blocks revealed by proton double-quantum NMR, *Macromolecules* **34,** 298–309 (2001).
11. D. Suwelack, W. P. Rothwell, and J. S. Waugh, Slow molecular motion detected in the NMR spectra of rotating solids, *J. Chem. Phys.* **73,** 2559–2569 (1980).
12. D. L. Vanderhart, W. L. Earl, and A. N. Garroway, Resolution in ^{13}C NMR of organic solids using high-power proton decoupling and magic-angle sample spinning, *J. Magn. Reson.* **44,** 361–401 (1981).
13. A. Schmidt, S. O. Smith, D. P. Raleigh, J. E. Roberts, R. G. Griffin, and S. Vega, Chemical exchange effects in the NMR spectra of rotating solids, *J. Chem. Phys.* **85,** 4248–4253 (1986).
14. J. R. Long, B. Q. Sun, A. Bowen, and R. G. Griffin, Molecular dynamics and magic angle spinning NMR, *J. Am. Chem. Soc.* **116,** 11950–11956 (1994).
15. M. S. Solum, K. W. Zilm, J. Michl, and D. M. Grant, Carbon-13 line shape study of two-site exchange in solid dimethyl sulfone, *J. Phys. Chem.* **87,** 2940–2944 (1983).
16. D. E. Favre, D. J. Schaefer, and B. F. Chmelka, Direct determination of motional correlation times by 1D MAS and 2D exchange NMR techniques, *J. Magn. Reson.* **134,** 261–279 (1998).
17. T. Gullion and J. Schaefer, Rotational-echo double-resonance NMR, *J. Magn. Reson.* **81,** 196–200 (1989).
18. M. Hong, Solid-state NMR determination of $^{13}C\alpha$ chemical shift anisotropies for the identification of protein secondary structure, *J. Am. Chem. Soc.* **122,** 3762–3770 (2000).
19. K. Schmidt-Rohr and H. W. Spiess, "Multidimensional Solid-State NMR and Polymers," Academic Press, London (1994).
20. H. Geen, J. J. Titman, J. Gottwald, and H. W. Spiess, Spinning sidebands in the fast-MAS multiple-quantum spectra of protons in solids, *J. Magn. Reson. A* **114,** 264–267 (1995).
21. J. Gottwald, D. E. Demco, R. Graf, and H. W. Spiess, High-resolution double-quantum NMR spectroscopy of homonuclear spin pairs and proton connectivities in solids, *Chem. Phys. Lett.* **243,** 314–323 (1995).
22. M. Feike, D. E. Demco, R. Graf, J. Gottwald, S. Hafner, and H. W. Spiess, Broadband multiple-quantum NMR spectroscopy, *J. Magn. Reson. A* **122,** 214–221 (1996).
23. K. Saalwächter, R. Graf, and H. W. Spiess, Recoupled polarization-transfer methods for solid-state ^{1}H-^{13}C heteronuclear correlation in the limit of fast MAS, *J. Magn. Reson.* **148,** 398–418 (2001).
24. K. Saalwächter and H. W. Spiess, Heteronuclear ^{1}H-^{13}C multiple-spin correlation in solid-state NMR: Combining REDOR recoupling and multiple-quantum spectroscopy, *J. Chem. Phys.* **114,** 5707–5728 (2001).
25. A. Schmidt and S. Vega, NMR line shape analysis for two-site exchange in rotating solids, *J. Chem. Phys.* **87,** 6895–6907 (1987).
26. Z. Luz, R. Poupko, and S. Alexander, Theory and dynamic magic angle spinning nuclear magnetic resonance and its application to carbon-13 in solid bullvalene, *J. Chem. Phys.* **99,** 7544–7553 (1993).
27. L. Frydman and B. Frydman, A novel approach for evaluating the NMR spectra of spinning solids: Application to the case of chemical exchange, *Magn. Reson. Chem.* **28,** 355–363 (1990).
28. J. H. Kristensen, H. Bildsøe, H. J. Jakobsen, and N. C. Nielsen, Theory and simulations of molecular dynamics in ^{2}H MAS NMR, *J. Magn. Reson.* **100,** 437–443 (1992).

29. M. Bak, J. T. Rasmussen, and N. C. Nielsen, SIMPSON: A general simulation program for solid-state NMR spectroscopy, *J. Magn. Reson.* **147,** 296–330 (2000).

30. R. R. Ernst, G. Bodenhausen, and A. Wokaun, "Principles of Nuclear Magnetic Resonance in One and Two Dimensions," Clarendon, Oxford, 1987.

31. S. Alexander, Exchange of interacting nuclear spins in nuclear magnetic resonance. II. Chemical exchange, *J. Chem. Phys.* **37,** 974–980 (1962).

32. G. Binsch, A unified theory of exchange effects on nuclear magnetic resonance line shapes, *J. Am. Chem. Soc.* **91,** 1304–1309 (1969).

33. T. Gullion, D. B. Baker, and M. S. Conradi, New, compensated Carr–Purcell sequences, *J. Magn. Reson.* **89,** 479–484 (1990).

34. D. Reichert, T. J. Bonagamba, and K. Schmidt-Rohr, Slow-down of ^{13}C spin diffusion in organic solids by fast MAS: A CODEX NMR study, *J. Magn. Reson.* **151,** 129–135 (2001).

35. Y. Ishii, J. Ashida, and T. Terao, ^{13}C–^{1}H dipolar recoupling dynamics in ^{13}C multiple-pulse solid-state NMR, *Chem. Phys. Lett.* **246,** 439–445 (1995).

36. A. E. Bennett, C. M. Rienstra, M. Auger, K. V. Lakshmi, and R. G. Griffin, Heteronuclear decoupling in rotating solids, *J. Chem. Phys.* **103,** 6951–6958 (1995).

37. G. Metz, X. Wu, and S. O. Smith, Ramped-amplitude cross polarization in magic-angle-spinning NMR, *J. Magn. Reson. A* **110,** 219–227 (1994).

38. A.-R. Grimmer, A. Kretschmer, and V. B. Cajipe, Influence of magic angle spinning on sample temperature, *Magn. Reson. Chem.* **35,** 86 (1997).

39. B. Langer, I. Schnell, H. W. Spiess, and A.-R. Grimmer, Temperature calibration under ultrafast MAS conditions, *J. Magn. Reson.* **138,** 182–186 (1999).

40. G.-J. M. P. van Moorsel, E. R. H. van Eck, and C. P. Grey, $Pr_2Sn_2O_7$ and $Sm_2Sn_2O_7$ as high-temperature shift thermometers in variable-temperature ^{119}Sn MAS NMR, *J. Magn. Reson. A* **113,** 159–163 (1995).

41. W. H. Press, B. P. Flannery, S. A. Teukolsky, and W. T. Vetterling, "Numerical Recipes in C," Cambridge Univ. Press, Cambridge, UK (1991).

42. I. Fischbach, "Festkörper-NMR-Spektroskopische Untersuchungen zur Dynamik in Hexabenzocoronenen," Diploma thesis, Universität Mainz, 2000.

43. Y. Yang, M. Schuster, B. Blümich, and H. W. Spiess, Dynamic magic-angle spinning NMR spectroscopy: Exchange-induced sidebands, *Chem. Phys. Lett.* **139,** 239–243 (1987).

44. V. Gérardy-Montouillout, C. Malveau, P. Tekely, Z. Olender, and Z. Luz, ODESSA, a new 1D NMR exchange experiment for chemically equivalent nuclei in rotating solids, *J. Magn. Reson. A* **123,** 7–15 (1996).

45. D. Reichert, H. Zimmermann, P. Tekely, R. Poupko, and Z. Luz, Time-reverse ODESSA: A 1D exchange experiment for rotating solids with several groups of equivalent nuclei, *J. Magn. Reson.* **125,** 245–258 (1997).

46. R. Tycko and G. Dabbagh, Measurement of nuclear magnetic dipole–dipole couplings in magic angle spinning NMR, *Chem. Phys. Lett.* **173,** 461–465 (1990).